iopscience.iop.org

Home Search Collections Journals About Contact us My IOPscience

Magnetostatic torsional actuator with embedded nickel structures for the improvement of driving force and wobble motion

This article has been downloaded from IOPscience. Please scroll down to see the full text article.

2011 J. Micromech. Microeng. 21 095007

(http://iopscience.iop.org/0960-1317/21/9/095007)

View the table of contents for this issue, or go to the journal homepage for more

Download details:
IP Address: 140.114.56.248
The article was downloaded on 09/03/2012 at 02:01

Please note that terms and conditions apply.

J. Micromech. Microeng. **21** (2011) 095007 (8pp) doi:10.1088/0960-1317/21/0/095007

Magnetostatic torsional actuator with embedded nickel structures for the improvement of driving force and wobble motion

Tsung-Lin Tang[1] **and Weileun Fang**[1,2]

[1] Power Mechanical Engineering, National Tsing Hua University, Hsinchu, Taiwan
[2] Institute of NanoEngineering and MicroSystems, National Tsing Hua University, Hsinchu, Taiwan

E-mail: fang@pme.nthu.edu.tw

Received 4 June 2011, in final form 26 June 2011
Published 29 July 2011
Online at stacks.iop.org/JMM/21/095007

Abstract
This study demonstrates the magnetostatic torsional actuator consisting in a Si–Ni compound frame to significantly improve the driving force. The present design has three merits: (1) it employs a Si mold to simultaneously electroplate/pattern thick Ni, and the Ni and Si structures respectively provide magnetostatic force and superior mechanical properties, (2) the embedded Ni structures not only increase the ferromagnetic material volume but also enhance magnetization strength to enlarge magnetostatic torque, (3) the Si–Ni compound structure, which is nearly symmetric about the torsional axis in the out-of-plane direction, can decrease the moment of inertia and also reduce the wobble motion. In applications, one-axis torsional actuator is implemented and characterized. The experiments show that the Si–Ni compound scanner has an optical scan angle $\theta_{\mathrm{optical}} = 90^\circ$ with the input power 81 mW. The input power is decreased as compared with the existing scanner. Moreover, the out-of-plane wobble motion is only 44 nm at $\theta_{\mathrm{optical}} = 15^\circ$. Compared with the existing designs consisted of asymmetric structures in the out-of-plane direction, such as electroplated film and silicon rib, about the torsional axis, the equivalent eccentric force is reduced nearly two-fold. In short, the proposed design not only increases the driving force but also decreases the wobble motion.

(Some figures in this article are in colour only in the electronic version)

1. Introduction

Presently microelectromechanical system (MEMS) technologies have found extensive applications in various areas. For instance, the characteristics of smaller feature size and lower power consumption make the MEMS sensors capable of being used in consumer applications [1–3]. The MEMS actuators, such as the linear and torsional actuators, are also promising and key devices for many consumer electronic products [4, 5]. The micro-torsional actuators play an important role in various micro-optical systems, for instance, the digital micromirror device [6], the micro-scanner [7] and the laser printer [8]. In general, the micro-torsional actuator for optical application consists of flexible springs, a stiff mirror plate and the driving components to modulate the incident light. Many driving components including the force-generating [9] and force-transmitting units [10] have been reported to improve the performance of the torsional actuator. The electrostatic and electromagnetic forces are two popular approaches to drive micro-torsional actuator [11–13]. However, the pull-in effect and electrical isolation are two critical designs considered for electrostatic torsional actuators. The electromagnetic force has an advantage to drive torsional actuators with large displacement. Presently, Lorentz force [12] and magnetostatic force [13] are the most common electromagnetic driving forces for torsional actuators.

In general, for the Lorentz force torsional actuator, the deposition of a conducting film is required for the electrical routing of the input current [12]. Moreover, deposition

 © 2011 IOP Publishing Ltd Printed in the UK & the USA

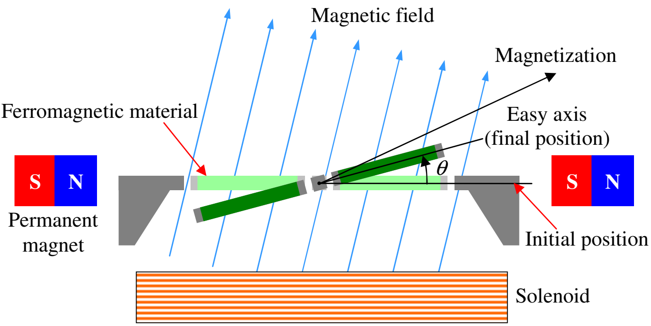

Figure 1. Actuation concepts of the torsional actuator driven by the magnetostatic force.

of the ferromagnetic film is required for the magnetostatic force torsional actuator [13]. A thicker ferromagnetic (or conducting) film can increase the torque applied on torsional actuators. However, the film thickness is limited to the fabrication process. Moreover, conducting and ferromagnetic films deposited on the surface of Si structures will introduce eccentric force and cause unwanted wobble motion [14]. The wobble motion of the torsional actuator may lead to problems for its applications, for instance, the reflective laser beam shake of micro-scanner [9]. The process on a double SOI (silicon on insulator) wafer has been employed to fabricate a torsional actuator with an axial symmetric structure to suppress the unwanted wobble motion [9]. Moreover, the design to drive the actuator by pure torque has also been reported to reduce the wobble motion [10].

This study presents the design and implementation of a torsional actuator driven by the magnetostatic force. The torsional actuator consists of a Si substrate with embedded thick Ni structures (Si–Ni compound), and the embedded Ni structures are patterned to a slender shape [15]. Thus, the volume and magnetization of ferromagnetic material increase significantly and the magnetostatic torque applied on the torsional actuator increases further. Moreover, the wobble motion of the torsional actuator is reduced since the Si–Ni compound structure is nearly symmetric about the torsional axis in the out-of-plane direction [16]. The fabrication processes have been established to realize the proposed torsional actuator. Moreover, measurements demonstrate the superior performance of the proposed actuator as compared with the existing ones. In applications, the optical scanners have been implemented to demonstrate the feasibility of the proposed design.

2. Concept and design

As illustrated in figure 1, a magnetostatic torque T will be applied on the torsional actuator after introducing a magnetic field H. The torque T is expressed as

$$T = V_{\mathrm{mag}} \cdot M \times H \tag{1}$$

where V_{mag} is the volume of ferromagnetic material embedded in the actuating frame and M is the magnetization. The permanent magnets near the torsional actuator are employed to specify the magnetization direction of ferromagnetic material.

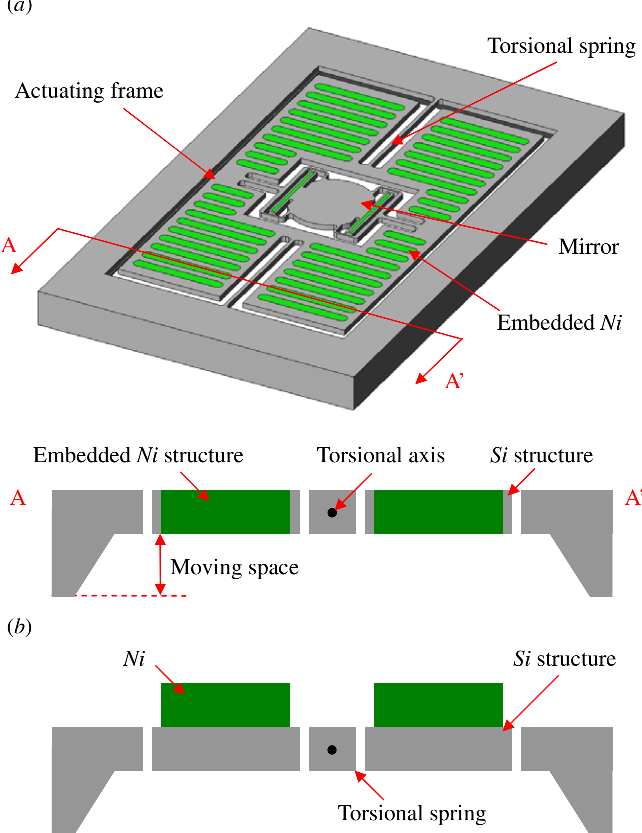

Figure 2. Design concepts. (*a*) Top view of the torsional actuation device, and A–A′ cross-section of Ni embedded inside the Si structure and (*b*) cross-section of existing design with Ni on the Si surface.

The magnetic field H is generated after applying the current to the solenoid. According to equation (1), the torque applying on the magnetostatic torsional actuator can be enlarged by increasing V_{mag} and M. This study employs the magnetostatic scanner in figure 2 to demonstrate the proposed design concept. As indicated in figure 2(*a*), the torsional actuator consists of the torsional springs, the actuating frame (Si–Ni compound structure) and the mirror plate. The ferromagnetic material of Ni is patterned to the slender shape and embedded in the thick Si to form the Si–Ni compound structure. Figure 2(*a*) also shows the A–A′ cross-section of the proposed design. The backside cavity on the Si substrate provides sufficient moving space for large scan angle operation. This study directly employs a patterned and etched Si substrate as the mold to electroplate the ferromagnetic material. Thus, the thick ferromagnetic material can be electroplated and embedded into the Si mold to increase V_{mag}. By using the patterned Si mold, the ferromagnetic material can also be electroplated to the slender shape to enhance the magnetization M. The proposed torsional actuator is then driven by the magnetostatic torque introduced by such a Si–Ni compound structure. As a result, the Si and Ni structures respectively provide their superior mechanical properties and magnetostatic characteristic. In comparison, the ferromagnetic material is electroplated and patterned on the surface of Si structures (on top electroplated Ni) [13], as shown in figure 2(*b*).

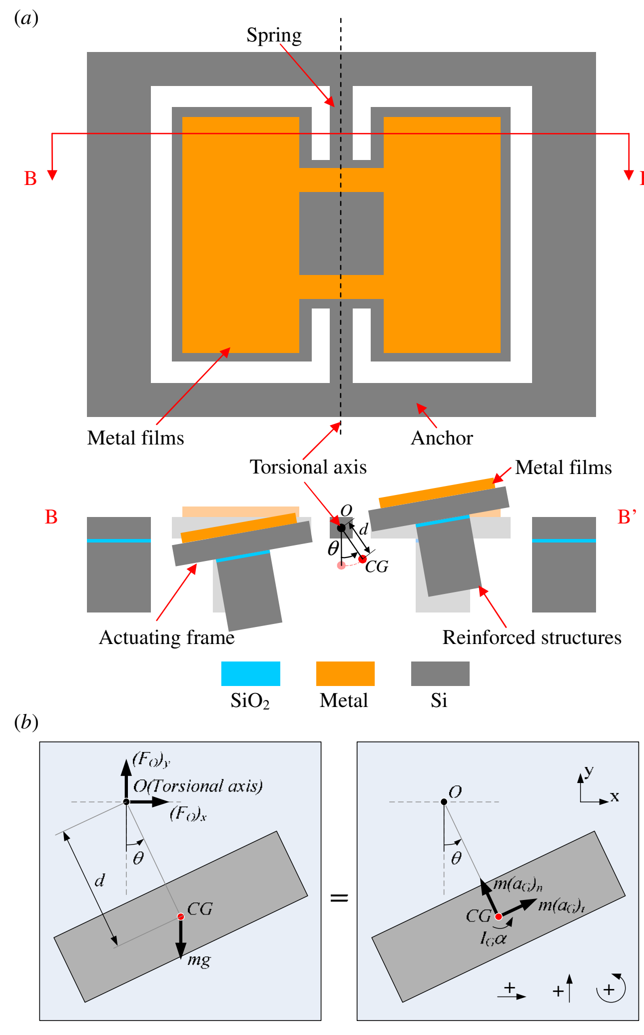

Figure 3. Analysis of the unwanted wobble motion induced by the eccentric force. (*a*) Top view and B–B′ cross-section of the typical dynamic model, and (*b*) free-body and kinetic diagrams of the angular-oscillating actuating frame.

As a typical dynamic model of the torsional actuator shown in figure 3(*a*), this study analyzes the unwanted wobble motion of an actuating frame introduced by the eccentric force during operation. The model indicates that either the front-side metal film (such as the electrical routings and magnetic layers [12, 13]) or the back-side reinforced structures [15] could lead to off-center mass as well as the eccentric force on the angular-oscillating actuating frame. The torsional actuator has an angular oscillation about the center O with a mechanical scan angle of $\pm\theta$. The angle θ can be expressed as

$$\theta = \theta_0 \sin(\omega_0 t) \tag{2}$$

where θ_0 is the maximum mechanical scan angle, ω_0 is the operation frequency of the torsional actuator. Thus, the angular velocity ω and angular acceleration α can be determined as

$$\omega = \omega_0\theta_0 \cos(\omega_0 t) \tag{3}$$

$$\alpha = -\omega_0^2\theta_0 \sin(\omega_0 t) \tag{4}$$

The equivalent center of gravity for the off-center mass in figure 3(*a*) has an offset of d (in the out-of-plane direction) to the torsional axis. The free-body and kinetic diagrams of the angular-oscillating actuating frame are further illustrated in figure 3(*b*). The centripetal acceleration $(a_G)_n$ and the tangential acceleration $(a_G)_t$ in the model can be expressed as

$$(a_G)_n = \omega^2 d \tag{5}$$

$$(a_G)_t = \alpha d \tag{6}$$

Thus, the actuating frame will introduce both in-plane force $(F_O)_x$ and out-of-plane force $(F_O)_y$ to the torsional spring. These forces can be expressed as

$$\begin{aligned}(F_O)_x &= m(a_G)_n \sin(\theta) - m(a_G)_t \cos(\theta)\\ &= md\omega_0^2\big(\theta_0^2\cos^2(\omega_0 t)\sin(\theta_0 \sin(\omega_0 t))\\ &\quad + \theta_0 \sin(\omega_0 t)\cos\big(\theta_0 \sin(\omega_0 t)\big)\big)\end{aligned} \tag{7}$$

$$\begin{aligned}(F_O)_y &= -mg - m(a_G)_n \cos(\theta) - m(a_G)_t \sin(\theta)\\ &= -mg - md\omega_0^2\big(\theta_0^2\cos^2(\omega_0 t)\cos(\theta_0 \sin(\omega_0 t))\\ &\quad - \theta_0 \sin(\omega_0 t)\sin(\theta_0 \sin(\omega_0 t))\big)\end{aligned} \tag{8}$$

Since the maximum mechanical scan angle θ_0 is only one-fourth of the optical one, these forces can be simplified by the approximate relations as follows:

$$\begin{aligned}&\sin(\theta_0 \sin(\omega_0 t)) \approx \theta_0 \sin(\omega_0 t)\\ &\cos(\theta_0 \sin(\omega_0 t)) \approx 1\end{aligned} \tag{9}$$

Moreover, the cubic term of θ_0 can be ignored. Thus, equations (7) and (8) can be rewritten as

$$(F_O)_x = md\omega_0^2\theta_0 \sin(\omega_0 t) \tag{10}$$

$$(F_O)_y = -mg - md\omega_0^2\theta_0^2 \cos(2\omega_0 t) \tag{11}$$

As a result, the magnitude of the time-varying eccentric force is proportional to both mass m and CG-offset d. The in-plane stiffness $(k_O)_x$ and out-of-plane stiffness $(k_O)_y$ of the torsional spring are respectively,

$$(k_O)_x = \frac{2Ew^3h}{L^3} \tag{12}$$

$$(k_O)_y = \frac{2Ewh^3}{L^3} \tag{13}$$

where E is the Young modulus of the spring, w is the spring width, h is the spring thickness and L is the spring length. After being subjected to the forces in equations (10) and (11), the equations of motion for the dynamic system shown in figure 3 can be expressed as

$$m\ddot{x} + c\dot{x} + (k_o)_x x = md\omega_0^2\theta_0 \sin(\omega_0 t) \tag{14}$$

$$m\ddot{y} + c\dot{y} + (k_o)_y y = -mg - md\omega_0^2\theta_0^2 \cos(2\omega_0 t) \tag{15}$$

where c is the damping constant of the dynamic system. The dynamic responses of $x(t)$ (in-plane wobble motion of actuating frame) and $y(t)$ (out-of-plane wobble motion of actuating frame) can be respectively expressed as

$$x(t) = \frac{md\omega_0^2\theta_0}{\left[\left((k_O)_x - m\omega_0^2\right)^2 + c^2\omega_0^2\right]^{1/2}} \sin(\omega_0 t - \phi_x) \tag{16}$$

Table 1. Comparisons of the Si–Ni compound structure and the on-top electroplated Ni design.

Items / Frame types	Moment of inertia (10^{-3} g · mm^2)			Off-axis of CG (μm)	Resonant frequency (Hz)
	Ni	Si	Total		
Si-Ni compound structure	5.81	1.90	7.71	0	690
On-top electroplated *Ni*	5.84	3.42	9.26	50	630

$$y(t) = -\frac{mg}{(k_O)_y} - \frac{md\omega_0^2\theta_0^2}{\left[\left((k_O)_y - 4m\omega_0^2\right)^2 + 4c^2\omega_0^2\right]^{1/2}} \times \cos(2\omega_0 t - \phi_y) \quad (17)$$

where the phase angles of ϕ_x and ϕ_y are,

$$\phi_x = \tan^{-1}\left(\frac{c\omega_0}{(k_O)_x - m\omega_0^2}\right) \quad (18)$$

$$\phi_y = \tan^{-1}\left(\frac{2c\omega_0}{(k_O)_y - 4m\omega_0^2}\right) \quad (19)$$

According to equation (17), the vibrating frequency of the out-of-plane wobble motion is twice the scanning frequency ω_0 of the actuating frame. In this study, the thicknesses of the Si structures (frame, spring and mirror) and the electroplated Ni are all 80 μm. Table 1 summarizes the characteristics of the proposed design and the one in figure 2(*b*). As compared with the design in figure 2(*b*), the proposed actuator can decrease the total moment of inertia to 83%. Moreover, the wobble motion induced by the off-axis of CG (center of gravity) is also reduced since the Si–Ni compound actuating frame is nearly symmetric about the torsional axis in the out-of-plane direction.

3. Fabrication and results

The magnetostatic torsional actuator with embedded Ni structures was implemented by using the process shown in figure 4. As indicated in figure 4(*a*), the thermal SiO_2 was grown on both sides of the Si substrate, and then the SiO_2 film at the backside of the Si substrate was patterned to define the window for bulk Si etching. After that, the Si substrate was etched by TMAH to define the thickness of the Si structure. As illustrated in figure 4(*b*), the Cr, Au and Ni layers were respectively deposited on the backside cavity of the Si substrate as the adhesion layer, seed layer and supporting layer. As shown in figure 4(*c*), the SiO_2 film at the front side of the Si substrate was patterned to act as the hardmask for the following dry etching, and then the DRIE process was used to define the area for Ni plating on the Si structure. After removing the Cr adhesion layer to expose the Au seed layer, the Ni structure embedded in the Si mold was electroplated. As depicted in figure 4(*d*), after striping

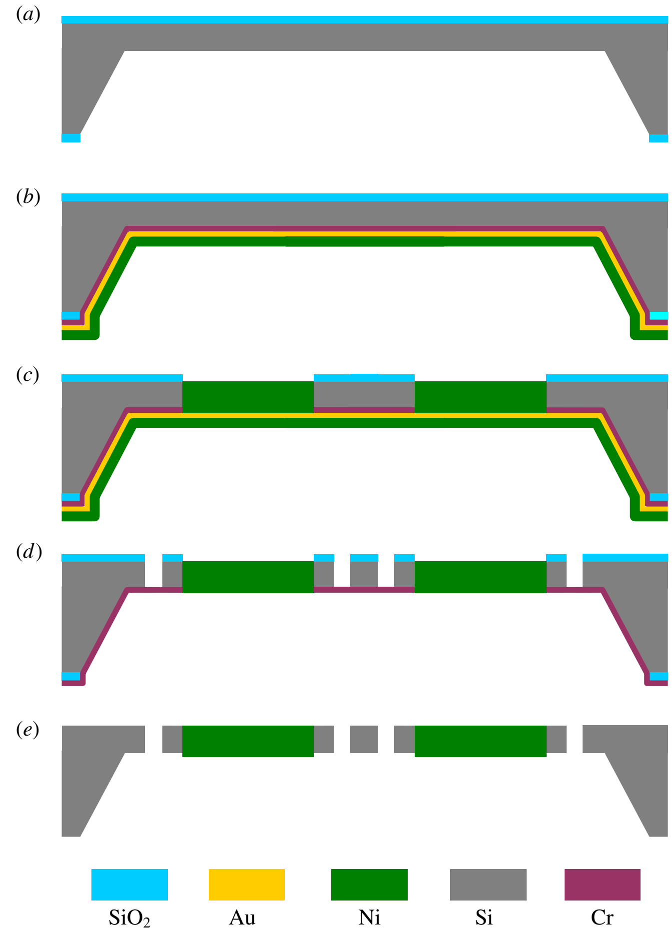

Figure 4. Fabrication process flow of the torsional actuator with embedded Ni structures.

the Ni supporting layer and Au seed layer from the backside of the Si substrate, the SiO_2 hardmask was patterned again and the following DRIE was used to define the shape of the Si mechanical structure. Finally, the Cr adhesion layer and SiO_2 were removed to release the device from the substrate, as shown in figure 4(*e*). Figure 5 further schematically illustrates the details regarding the implementation of the embedded Ni structure. As indicated in figure 5(*a*), the SiO_2 on the top of the Si structures acts as a hard mask. The Cr adhesion layer, Au seed layer and Ni supporting layer were respectively deposited on the back side of the Si structures. As shown in figure 5(*b*), the Si acting as a mold for Ni electroplating was defined by DRIE, and then the Cr adhesion layer was patterned by wet etching. The Au seed layer in this study was only 0.2 μm thick. Hence, the suspended thin Au seed layer would easily be damaged during the following fabrication processes. In this regard, the Ni supporting-layer (15 μm) was employed to support and protect the thin seed layer. After the electroplating process in figure 5(*c*), the bulk electroplated Ni material was embedded in the Si mold structure. This method can avoid the problems induced by the non-uniformity of the seed layer deposited on the Si mold, and the plating voids and pinch-off problems for deep cavity plating [17].

In comparison, the torsional actuator in figure 2(*b*) was also implemented by the process shown in figure 6. As

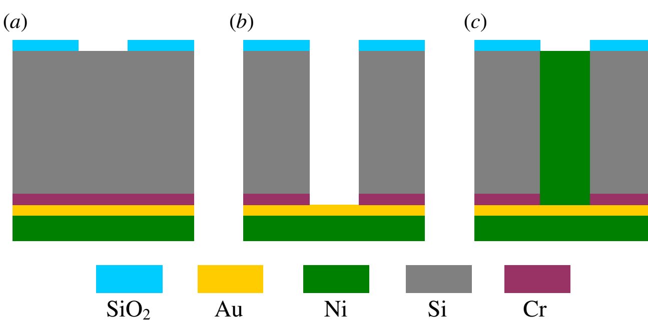

Figure 5. Details about the implementation of the embedded Ni structure.

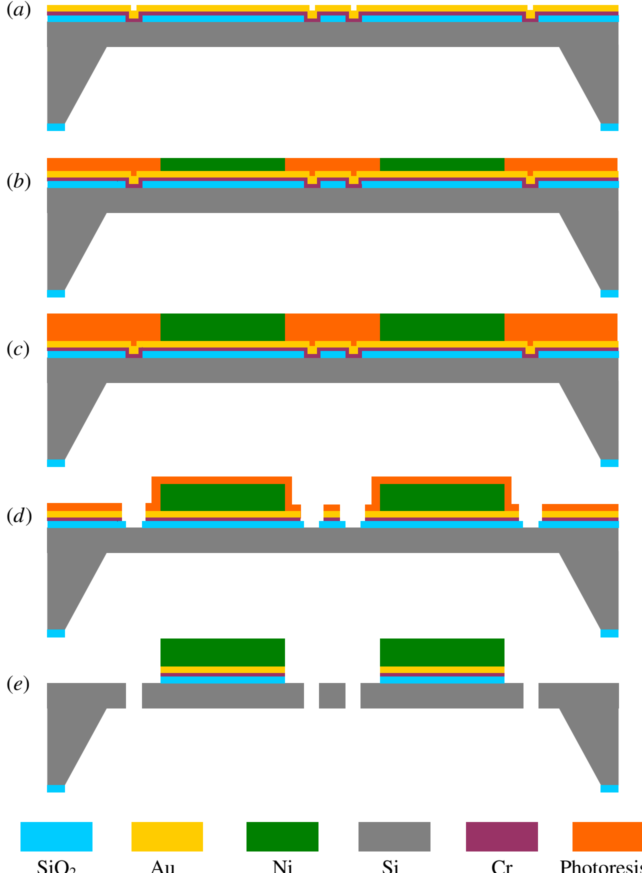

Figure 6. Fabrication process flow of the existing design with Ni structures on the surface of Si structures (on-top Ni design).

shown in figure 6(*a*), the thermal SiO_2 was deposited and patterned on the backside of the Si substrate for TMAH bulk etching. After that, the topside SiO_2 was patterned as the hardmask for the following DRIE. The Cr and Au layers were respectively deposited on the topside Si substrate as the adhesion layer and seed layer. As illustrated in figure 6(*b*), a 40 μm thick photoresist (AZ4620) acted as a mold after photolithography, and then the thick Ni was electroplated and molded. Figure 6(*c*) shows the second molding process without stripping the photoresist in the previous step. The two-step electroplating process enabled the Ni layer to become 80 μm thick. As shown in figure 6(*d*), after stripping the photoresist, a 13 μm thick photoresist was coated on the 80 μm thick Ni structures and patterned to define the Cr and Au layers. Finally, the DRIE was used to define and release the Si structures, and the photoresist, Au, Cr and SiO_2 layers were removed, as shown in figure 6(*e*).

The SEM (scanning electron microscopy) micrographs in figures 7(*a*) and (*b*) show the front side and backside of a typical fabricated torsional actuator. The mirror, Si–Ni compound structures and torsional springs are observed. The frame is embedded with the slender Ni structures to increase the magnetostatic torque. The zoom-in micrographs in figures 7(*c*) and (*d*) respectively show the top and cross-sectional views of the Ni–Si compound structures. It is clearly observed that the electroplating Ni was successfully molded and patterned by the Si structures. The Si frame and the embedded Ni structure are near 80 μm thick, and the aspect ratio of the presented Ni structure is 2. Figure 7(*e*) shows the existing design with on-top electroplated Ni (as illustrated in figure 6(*e*). The side view micrograph in figure 7(*f*) shows the two-step electroplating for 80 μm thick Ni.

4. Experiments and discussions

In applications, a micro-scanner driven by the presented magnetostatic torsional actuator is demonstrated. As shown in figure 8(*a*), a 5 mm × 8 mm Si chip containing the micro-scanner and the micro-actuator is assembled with the permanent magnets and the solenoid on a plastic stage. The permanent magnets are employed to specify a magnetic field to ensure the magnetization direction of the embedded Ni structures. The solenoid embedded inside the plastic stage provides a periodic magnetic field to actuate the scanner. Figure 8(*b*) shows the driving test of the scanner in a measurement stage to characterize the scan angle. The incident green laser beam was focused on the scanner through the window of the testing stage. After that, the reflective laser beam was projected to the curved screen, and the optical scan angle was read directly from the scale on stage. Typical test results show that the presented scanner in figure 7(*a*) has an optical scan angle of $\theta_{\text{optical}} = 90^\circ$ when operated at its resonant frequency of 619 Hz with an input power of $P_{\text{input}} =$ 81 mW. In comparison, the scanner in [13] was operated at the resonant frequency of 367 Hz with an optical scan angle of $\theta_{\text{optical}} = 88^\circ$ using 170 mW input power. Despite the presented scanner having a stiffer torsional stiffness, it requires a much smaller input power when driving at the same scan angle. Measurements in figure 9 show the dynamic responses of the scanner characterized by laser Doppler vibrometer. As indicated in figure 9, the laser spot was focused on position A (position A is on the nodal line of the scanning mode) to detect the out-of-plane wobble motion of the actuating frame. In addition, the laser spot was focused on position B to characterize its scan angle. As limited by the numerical aperture of objectives, the measurements are only available for small scan angles. As the scanner is scanned with an optical angle of $\theta_{\text{optical}} = 15^\circ$, the out-of-plane wobble of the actuating frame is 44 nm. Note that the excitation introduced by the periodic eccentric force has a frequency double the

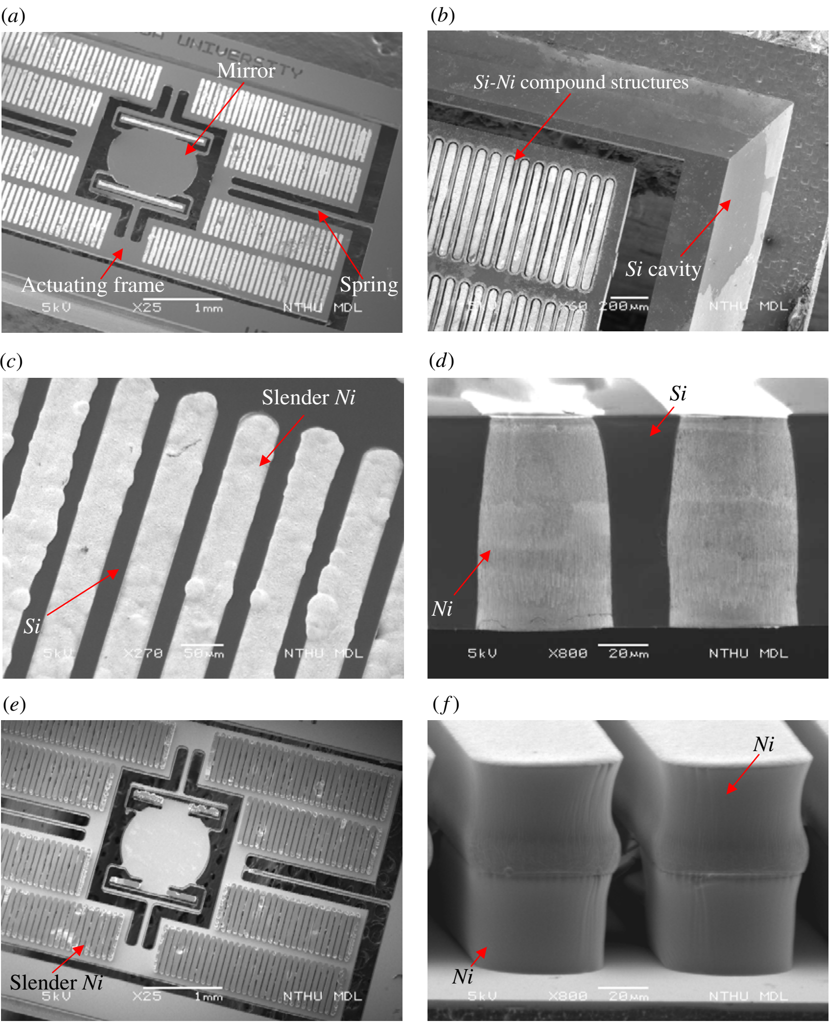

Figure 7. SEM micrographs of (*a*) front side and (*b*) backside of a typical fabricated torsional actuator with embedded Ni structures, (*c*) and (*d*) top and cross-section of Si–Ni compound structures, (*e*) front side of existing design with slender Ni structures on Si surface and (*f*) two step electroplating of slender Ni structures.

mirror scanning frequency. Thus, the frequency of the wobble motion is double the scanning frequency.

In comparison, the existing torsional actuator designs as shown in figure 2(*b*) have also been fabricated (with two different thicknesses, 40 and 80 μm, of electroplated Ni) and tested. To make a fair comparison, these actuators have the same torsional stiffness. The actuators were driven at the following two conditions: (1) with the same input power $P_{\text{input}} = 81$ mW and (2) with the same optical scan angle $\theta_{\text{optical}} = 15^\circ$. The measurement results of the optical scan angle and out-of-plane wobble displacements are summarized in table 2. As indicated in table 2, the optical scan angle is increased from 65° to 90° (i.e. 138%) at the same input power when the thickness of Ni structures increases from 40 to 80 μm. It shows the thickness of the Ni structure successfully increases the optical scan angle and further increases the driving force. Furthermore, table 2 also shows that the wobble displacement of the proposed design is only 44 nm. However, the scanners with on-top electroplated Ni have a larger wobble displacement. The wobble displacement of the proposed design is mainly induced by the thickness deviation of the electroplated Ni. The wobble displacement of the scanner with on-top electroplated Ni is reduced from 76 to 52 nm when the thickness of the electroplated Ni film is decreased from 80 to 40 μm. Comparing the scanners with the same Ni thickness, the wobble displacement is decreased to 58% by the proposed embedded Ni design. Note that the torsional actuators discussed in table 2 are operated at their resonant frequency of nearly 600 Hz. According to equation (17), the out-of-plane wobble motion is proportional to the square of the driving frequency. Thus, the scanner could have a much larger wobble motion as the driving frequency is increased.

Moreover, the existing scanner in [15] has also been tested for comparison with the proposed design, as shown in table 3. The wobble displacement of the existing scanner in [15] is 720 nm. Since the scanners in table 3 have different spring stiffness, the time-varying equivalent eccentric force can be determined by equation (17) for a fair comparison. As indicated in table 3, the eccentric force of the existing scanner in [15] is 3.39×10^{-5} N, whereas the proposed design is only

(*a*)

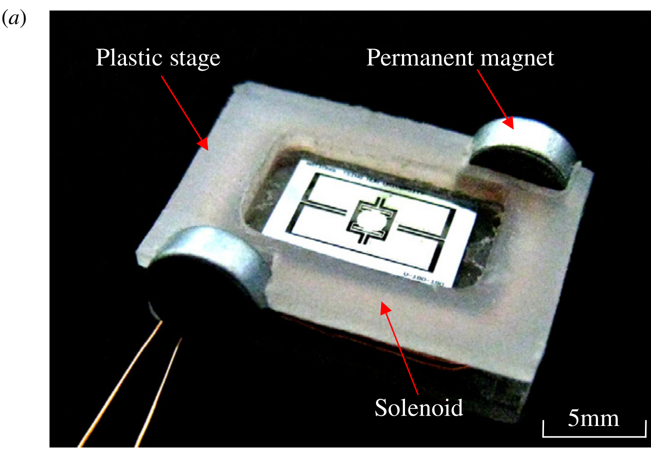

(*b*)

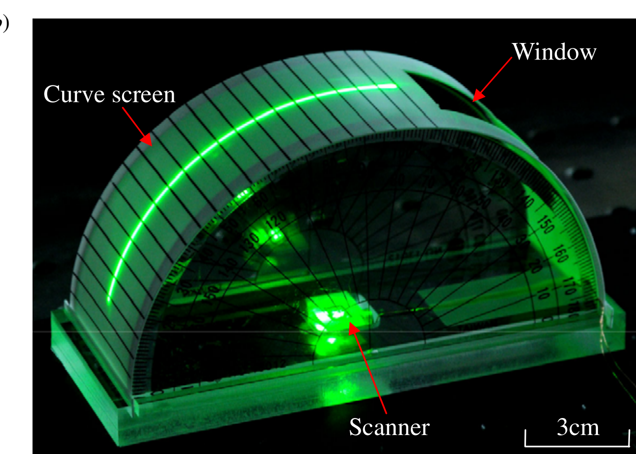

Figure 8. Experimental setup. (*a*) Driving stage and (*b*) optical scan angle measurement stage.

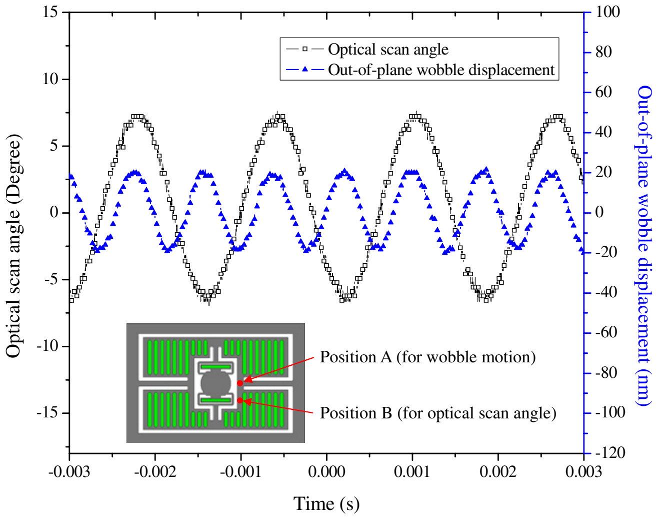

Figure 9. Dynamic responses of the out-of-plane wobble motion.

1.70×10^{-5} N. Therefore, the results show that the embedded Ni structure design decreases the equivalent eccentric force by 50%. In conclusion, the present design not only increases the driving force but also suppresses the wobble motion.

Table 2. Measurement results of the scanners with the embedded Ni design and the on-top Ni of two different thicknesses.

Devices \ Items	Optical scan angle with P_{input} = 81mW (Degree)	Resonant frequency of scanning mode (Hz)	Wobble displacement at $\theta_{optical}$ = 15° (nm)
On top 80μm *Ni*	90	533	76
On top 40μm *Ni*	65	607	52
Embedded 80μm *Ni*	90	619	44

Table 3. Comparison of the measured eccentric forces respectively from the existing scanner and from the proposed embedded Ni design.

Devices \ Items	Wobble displacement (nm)	Out-of-plane stiffness (N/m)	Equivalent eccentric force (N)
Existing scanner in [15]	720	1.81×10^{2}	3.39×10^{-5}
Embedded 80μm *Ni*	44	8.03×10^{2}	1.70×10^{-5}

5. Conclusion

This study presents a magnetostatic torsional actuator design consisting of a novel Si–Ni compound structure as the actuating frame. This study establishes the process to apply the Si substrate as a mold for Ni electroplating to implement the torsional actuator with the Si–Ni compound actuating frame. The Si–Ni compound structure with thick and slender Ni structures is designed to increase the volume and magnetization of the ferromagnetic material. Thus, the driving torque for the magnetostaitc torsional actuator is significantly improved. Typical test results show that the presented scanner with the 80 μm thick Si–Ni actuating frame has an optical scan angle of $\theta_{\text{optical}} = 90°$ when operated at its resonant frequency of 619 Hz with an input power of 81 mW. The input power has been decreased by two-fold (from 170 to 81 mW) in comparison to the existing scanner design. Moreover, the actuating frame consisted of the Si–Ni compound structure is nearly symmetric about the torsional axis in the out-of-plane direction, and thus the wobble motion is significantly reduced. In comparison, the existing torsional actuators with on-top electroplated Ni are fabricated and tested. The equivalent eccentric force is reduced by two-fold (from 3.39×10^{-5} to 1.70×10^{-5} N).

Acknowledgments

This paper is based (in part) upon work supported by the National Science Council, Taiwan under Grant NSC

98-2221-E-007-003-MY3, and by the Ministry of Economic Affairs, Taiwan, under contract no 98-EC-17-A-07-S1-011. The authors would like to express their appreciation to the Nano Science and Technology Center of National Tsing Hua University, and Nano Facility Center of National Chiao Tung University in providing the fabrication facilities.

References

[1] Yazdi N, Ayazi F and Najafi K 1998 Micromachined inertial sensors *Proc. IEEE* **86** 1640–59
[2] Eaton W P and Smith J H 1997 Micromachined pressure sensors: review and recent developments *Smart Mater. Struct.* **6** 530–9
[3] Scheeper P R, van der Donk AG H, Olthuis W and Bergveld P 1994 A review of silicon microphones *Sensors Actuators* A **44** 1–11
[4] Gutierrez R C, Tang T K, Calvet R and Fossum E R 2007 MEMS digital camera *Proc. SPIE* **6502** 65020K
[5] Scholles M, Bräuer A, Frommhagen K, Gerwig C, Lakner H, Schenk H and Schwarzenberg M 2008 Ultracompact laser projection systems based on two-dimensional resonant microscanning mirrors *J. Micro/Nanolithography, MEMS, MOEMS* **7** 021001
[6] Van Kessel P F, Hornbeck L J, Meier R E and Douglass M R 1998 A MEMS-based projection display *Proc. IEEE* **86** 1687–704
[7] Tauscher J, Davis W O, Brown D, Ellis M, Ma Y, Sherwood M E, Bowman D, Helsel M P, Lee S and Coy J W 2010 Evolution of MEMS scanning mirrors for laser projection in compact consumer electronics *Proc. SPIE* **7594** 75940A
[8] Davis W O, Brown D, Helsel M, Sprague R, Gibson G, Yalcinkaya A and Urey H 2007 High-performance silicon scanning mirror for laser printing *Proc. SPIE* **6466** 64660D
[9] Mizoguchi Y and Esashi M Design and fabrication of a pure-rotation microscanner with self-aligned electrostatic vertical combdrives in double SOI wafer *Digest Tech. Papers Transducers'05 conf., (Seoul, June 2005)* pp 65–86
[10] Lin H-Y and Fang W 2003 A rib-reinforced micro torsional mirror driven by electrostatic torque generators *Sensors Actuators* A **105** 1–9
[11] Hsu S, Klose T, Drabe C and Schenk H 2008 Fabrication and characterization of a dynamically flat high resolution micro-scanner *J. Opt.* A **10** 044005
[12] Yalcinkaya A D, Urey H, Brown D, Montague T and Sprague R 2006 Two-axis electromagnetic microscanner for high resolution displays *J. Microelectromech. Syst.* **15** 786–94
[13] Yalcinkaya A D, Urey H and Holmstrom S 2007 Ni–Fe plated biaxial MEMS scanner for 2-D imaging *IEEE Photonics Technol. Lett.* **19** 330–2
[14] Seren H R, Ferhanoglu O, Hatipoglu G, Boyman M, Olcer S, Ataman C and Urey H 2009 Miniaturized FR4 spectrometers *Int. Symp. on Optomechatronic Technologies, (Istanbul)* pp 158–63
[15] Tang T-L, Shu C-P, Chen W-C and Fang W 2010 Design and implementation of a torque-enhancement 2-axis magnetostatic SOI optical scanner *J. Micromech. Microeng.* **20** 025020
[16] Tang T-L, Chen R and Fang W 2011 Magnetostatic torsional actuator with embedded nickel structures for pure rotation *Int. Conf. on Micro Electro Mechanical Systems, (Cancun, Mexico 2011)* pp 1249–52
[17] Malta D, Gregory C, Temple D, Wang C, Richardson T and Zhang Y 2009 Optimization of chemistry and process parameters for void-free copper electroplating of high aspect ratio through-silicon vias for 3D integration *Electronic Components and Technology Conf., (San Diego)* pp 1301–6